Examining the adsorption of gases into solid crystalline molecular copper (II) 3,5-bis(trifluoromethyl)benzoate derivatives

Oriol Vallcorba [a], Julio Fraile-Sainz [b], Concepción Domingo [b], José A. Ayllón [c,*]

[a] ALBA Synchrotron Light Source, 08290, Cerdanyola del Vallés, Barcelona, Spain
[b] Instituto de Ciencia de Materiales de Barcelona (CSIC), Campus UAB, 08193, Bellaterra, Spain
[c] Departamento de Química, Universidad Autónoma de Barcelona, 08193, Bellaterra, Barcelona, Spain

A R T I C L E   I N F O

A B S T R A C T

Two copper(II) complexes, both involving the anionic 3,5-bis(trifluoromethyl)benzoate ligand (TFMBz), have been prepared and their structure elucidated by single crystal-X ray diffraction. $[Cu(TFMBz)_2(ISNA)_2]$ (**1**) is a mononuclear complex, in which the sphere of coordination of Cu(II) is completed by two neutral isonicotinamide (ISNA) auxiliary ligands. Hydrogen bonding formed between auxiliary ISNA ligands determines the formation of a 2D supramolecular network. $[Cu_2(TFMBz)_4(DMSO)_2]$ (**2**) is a binuclear complex, in which the four carboxylate ligands define the typical paddle wheel structure often found in copper complexes, containing also the ancillary dimethyl sulfoxide (DMSO) ligand in axial positions. The elucidated crystallographic data provide the static view of the crystal structures, which reveals only non-interconnected voids for both materials. Even that, compound **1** shows an appreciable adsorption of CO_2 at 273 K (*ca.* 1 CO_2 molecule/Cu atom at 100 kPa), concomitant with a reduced adsorption of Ar or N_2 under similar conditions, which implies a considerable degree of selectivity for CO_2. Moreover, **1** does not adsorb N_2 or Ar at 77 K and 100 kPa. This behavior suggests that the stablished intermolecular hydrogen bonds rest flexibility and dynamism to **1** at low temperature. Contrarily, increasing the temperature transient porosity is originated, which allows guest molecules to diffuse through the cavities. Compound **2** shows adsorption of N_2 and Ar at 77 K, indicating that vibrations in the network and rotation of some CF_3 groups, necessary to favor adsorbate diffusion, are still feasible at this low temperature.

1. Introduction

Microporous materials have been the object of considerable research due to the key roles that their pores play in many industrial processes. Although at industrial level the use of materials based on microporous carbonaceous materials and zeolites is still highly predominant, several alternative emergent microporous compounds are reaching interest. Among them, metal-organic frameworks (MOFs) are being explored in deep, due to the large number of parameters that can be chosen to tune the properties of their pores, thus given place to thousands of different materials [1–3]. Covalent organic frameworks (COFs) [4,5] form another family of microporous materials based in pure organic precursors. Both kind of materials, MOFs and COFs, have in common a structure based on a polymeric network, usually bi or tridimensional, defined by strong covalent bonds, including coordination bonds in MOFs.

An important, but less researched, area is the study of microporous materials based on discrete (instead of polymeric) units, which has recently gained considerable attention to shape highly functional porous material. The development of this class of materials is still in an early stage, with even no consensus in their terminology, interchangeably receiving the name of porous molecular crystals (PMCs) [6–8], nanoporous molecular crystals (NMCs) [9], hydrogen bonded organic frameworks (HOFs) [10], hydrogen bonded organic-inorganic frameworks (HOIFs) [11], and so on. The different terms are used to emphasize the nature of the discrete molecular units (organic or organometallic, *i.e.*, coordination complexes) and/or to indicate the type of intermolecular forces that connect the molecular units in the solid state. Along this work, the newly synthetized compounds are named as PMCs, which we considered a comprehensive denomination. The principal advantage of PMCs is solution processability, so the material can be redissolved for guest release and/or recrystallized for further reutilization. There are some examples of described PMCs with noticeable surface area [12], potential for noble gasses separation and enantioselective

---

partitioning [13], or even responsiveness to external stimuli [14]. The porosity in PMCs may have different origins. In some cases, extrinsic porosity is derived from the inefficient packing of intrinsically non-porous molecules [15], while other PMCs are straightforwardly built from intrinsically porous molecules, usually named as cages. When the packing of these cages is inefficient, the resulting material has two sources of porosity, intrinsic and extrinsic [16,17]. Moreover, some molecular materials without intrinsic voids but presenting adsorption in contact with specific guest molecules have been described [18]. These materials are prone to structural modifications, forced by the presence of the adsorbate, which generate pores and allows adsorption. These substances are known as switching adsorbent molecular materials [19].

To attain PMCs built from intrinsically non-porous molecules, the shape of the molecules is a key aspect, as some molecular geometries are more prone to inefficient packing during crystallization than others [20–23]. However, the packing behavior is hard to anticipate, as intermolecular forces (hydrogen bonding, π-π interactions and all sort of weak interactions) are also crucial in dictating the growth of the supramolecular network by crystallization.

In intrinsically porous PMCs, the molecular units can either pack to give a permanent interconnected porous structure or reveal the existence of isolated, guest inaccessible, voids [24]. It is worth mentioning that usually porosity analyses are performed from the static perspective given by crystal structure data, not accounting by molecular vibrations and rotation movements. For this reason, experimental adsorption data can noticeably differ from that simulated from structural data. As a result, in some cases certain guest molecules can experimentally diffuse inside a material structurally defined as nonporous. Hence, to understand the physicochemical properties of these materials it becomes necessary to take into account the dynamic porosity, since, under proper experimental conditions, molecular and lattice flexibility can produce "transient" channels that allow the diffusion of adsorbates through the host solid crystal structure [24–26]. Dynamic motion of some atoms or molecular constituents of the solid host framework must be considered to understand in which way the pores become interconnected to allow adsorbate diffusion. This phenomenon has been termed by Barbour and others as "porosity without pores" [27,28]. The necessary flexibility in the molecules forming the solid framework is activated thermally or with other external stimuli, such as pression. In PMCs, the supramolecular network flexibility is favored by the fact that the discrete building units are only connected by weak intermolecular forces.

Clearly, the understanding of the diffusion of guests within porous molecular solids needs to be increased to design new materials for specific applications. Hence, the main aim of this work is to contribute to the interpretation of these materials based on the analysis of two specific products involving bis(trifluoromethyl)benzoate (TFMBz)₂ and Cu(II). Molecular units including the TFMBz ligand are prone to show inefficient packing due to the disposition of the two voluminous trifluoromethyl groups. This behaviour has previously been observed and reported for three different Co(II) 1D coordination polymers containing this benzoate ligand [29]. In this work, two molecular Cu(II) complexes including TFMBz ligand and two different ancillary ligands (dimethylsulfoxide (DMSO) and isonicotinamide (ISNA)) are synthetized and described in regard of the crystal structure. N₂, Ar and CO₂ adsorption experiments at different temperatures were performed to determine which potential guest and at what temperature can diffuse into the voids of the solid material.

2. Experimental section

2.1. Materials

Copper(II) acetate hydrate (Cu(CH₃COO)₂·H₂O), 3,5-bis(trifluoromethyl)benzoic acid (HTFMBz), ISNA, DMSO and methanol were purchased from commercial sources and used as received.

2.2. Synthesis

2.2.1. Synthesis of [Cu(TFMBz)₂(ISNA)₂] (1)

HTFMBz (1.032 g, 4.00 mmol) and Cu(CH₃COO)₂·H₂O (0.399 g, 6.02 mmol) were dissolved in methanol (100 mL) and, then, the proper amount of ISNA (0.500 g, 4.09 mmol) was added. The resulting blue solution was concentrated at room temperature in a laboratory hood until a blue-lavender solid crystallized. The solid was filtered, washed twice with a small volume of methanol (2x5 mL) and dried on air. Yield was about 75 wt%. E.A. calcd. (wt%) for $C_{30}H_{18}O_6N_4F_{12}Cu$ (822.0 g mol⁻¹): C, 43.83; H, 2.21; N, 6.82. Found: C, 43.93; H, 2.21; N, 6.56.

2.2.2. Synthesis of [Cu₂(TFMBz)₄(DMSO)₂] (2)

HTFMBz (1.032 g, 4.00 mmol) and Cu(CH₃COO)₂·H₂O (0.399 g, 6.02 mmol) were added to DMSO (50 mL) and the suspension was heated to boiling. During this process, the initial greenish solution, with some solid in suspension, gave place to a blue solution. On standing at room temperature, a blue crystalline solid precipitated, which was filtered, washed twice with a small volume of methanol (2x5 mL) and dried on air. The yield was about 87 wt%. E.A. calcd. (wt%) for $C_{40}H_{24}O_{10}F_{24}S_2Cu_2$ (1311.8 g mol⁻¹): C, 36.62; H, 1.84. Found: C, 36.63; H, 1.80.

2.3. Characterization methods

Samples chemical composition was assessed by elemental analysis (E.A., Thermo Carlo Erba Flash 2000). Powder X-ray diffraction patterns (PXRD) were recorded at room temperature in a Siemens D5000 diffractometer, using the Cu Kα incident radiation. Synchrotron powder X-ray diffraction (SPXRD) measurements were performed at the BL16-NOTOS beamline of the ALBA synchrotron. Data were collected at 20 keV (0.62074 Å wavelength) in the transmission mode using the Mythen-II detector (6 modules at 535 mm from the sample). The powdered sample was placed inside of an *ad hoc* capillary reaction cell made of a fused silica capillary with 0.7 and 0.85 mm inner and outer diameters, respectively. The capillary was connected to both a gas-handling and a vacuum line. An Oxford Cryostream 700 instrument was used to control the temperature of the sample. Differential scanning calorimetry (DSC) experiments were performed under N₂ atmosphere in a dynamic Mettler Toledo DSC 821e equipment. A thermal heat program was settled consisting in cooling the sample from 25 to - 140 °C at a cooling rate of 5 °C min⁻¹. After 1 min at this temperature, the reverse heating at the same rate was performed. Molar enthalpies of transition (Δ*H*) were calculated from peak areas using original software provided by Mettler Toledo. The gas adsorption behavior was determined at either 77 or 273 K with N₂, Ar and CO₂ probe gasses using an ASAP 2000 Micromeritics Inc apparatus. Samples were first degassed at 373 K during 20 h.

2.4. Crystal structures

The crystal structures of **1** and **2** were solved using synchrotron single-crystal XRD (SSCXRD) data collected in the XALOC beamline of the ALBA Synchrotron [30]. Measurements were performed at 100 K with a 0.72929 Å wavelength using the Dectris Pilatus 6 M detector placed at 120 mm from the sample. Three sets of 360° φ-scans (in steps of 0.5° and 0.15 s·step⁻¹) at three κ angles (0, 45 and 90°) were attempted and the successful ones were merged afterwards to increase data completeness and redundancy. Data were indexed, integrated and scaled using XDS software [31]. The crystal structures were solved by intrinsic phasing and refined with SHELXL [32] by full-matrix least-squares methods on F² (version 2014/7) using Olex2 as the graphical interface [33]. Hydrogen atoms bonded to carbon atoms were placed in calculated positions with isotropic displacement parameters fixed at 1.2 times the U_eq of the corresponding carbon atoms. Data for compound **2** was also taken at room temperature using Mo Kα radiation (λ = 0.71073 Å)

in a SMART-APEX diffractometer with a CCD detector. An empirical absorption correction was applied (SADABS) and was solved and refined using the same procedure described previously. The crystallographic data and refinement details for both compounds are summarized in Tables S1–S5 of the SI.

CCDC 2240642–2240644 files contain the supplementary crystallographic data for this paper. These data can be obtained free of charge *via* www.ccdc.cam.ac.uk/data_request/cif.

3. Results and discussion

3.1. Synthesis and basic characterization

In this work, two molecular solids were prepared by exchange reactions in solution, in which the acetate present in the precursor was replaced by the TFMBz ligand with the concomitant addition of ancillary neutral ligands ISNA or DMSO and the subsequent crystallization of [Cu(TFMBz)$_2$(ISNA)$_2$] (**1**) and [Cu$_2$(TFMBz)$_4$(DMSO)$_2$] (**2**), respectively. The synthesis of both compounds is straightforward from the HTFMBz and Cu(II) acetate reagents. The synthesis of (**1**) was carried out at room temperature in methanol, which is a good solvent for both main reagents and the ISNA ancillary ligand. Compound (**2**) was synthetized in DMSO, solvent that was incorporated to the structure as axial ligand. In the later, a small amount of an amorphous unknown insoluble intermediate was formed at room temperature, reason why the mixture was heated to boiling to assure the complete dissolution of the precursors. The desired product crystallized on cooling. The elucidated crystal structure by SSCXRD for these compounds is described in the next section. Phase purity of the different precipitated compounds was first confirmed by E. A., in which obtained C,H,N values matched the given stoichiometry in both cases. Second, PXRD patterns recorded and simulated from single crystal data were compared displaying perfect coincidence (Figs. S1–S2). Finally, the retention of crystallinity upon gas sorption and desorption was confirmed by PXRD.

3.2. Structures

3.2.1. Structure of [Cu(TFMBz)$_2$(ISNA)$_2$] (1)

Compound **1** belongs to the triclinic crystal system, with the space group P-1. The asymmetric unit contains a Cu(II) atom, located at an inversion center, a TFMBz anion, and one ISNA ligand. In this mononuclear complex, two equivalent TFMBz ligands coordinate the metal center in a strongly asymmetrical quelating mode (Cu-O distances of 1.9764(14) and 2.5493(16) Å). The plane of the aromatic ring of the

TFMBz ligand are slightly tilted (7.15(10)°) respect the CuO$_4$ plane. The distorted octahedral geometry around each metal ion is completed by two pyridinic nitrogen atoms from two equivalent ISNA ligands (Cu-N 1.9942(18) Å). The plane defined by the aromatic ring of ISNA is almost orthogonal to the CuO$_4$ plane (dihedral angle 89.96(9)°) (Fig. 1a). The amide group of each ISNA establishes intermolecular hydrogen bonds that connect two close ISNA ligands belonging to two different molecules (Fig. 1b, Table 1). One of the H atoms of each amide group is hydrogen bonded to the O of the amide group of a neighbor ligand (N(2)-H(2A)⋯O(3)). These hydrogen bonds create the typical supramolecular symmetric amide-amide synthon [34,35]. Besides, the other H in each amide group is connected to one O atom of a carboxylate group in a TFMBz belonging to a third molecule (N(2)-H(2B)⋯O(2)). This connection is reinforced by another contact between this O and one of the H atoms of the aromatic ring of ISNA (C(12)-H(12)⋯O(2)). Therefore, each molecular subunit is connected by hydrogen bonds to another four, two through each ISNA ligand. The expansion of these contacts generates supramolecular layers parallel to de *ab* plane (Fig. 1c). In these layers, the TBMBz ligand protrude (Fig. 1d) and when the layers stack, they interdigitate. The strongest inter-layer interactions are stablished between the H of the aromatic ring at *para* position and the O of the amide group of a close by layer, C(12)-H(12)⋯O(2) (Fig. 1e and f). Fluoride atoms do not participate in any remarkable intermolecular interaction. This 3D packing determines non-interconnected voids, which accounts for a 9.3% of the crystal cell volume when measured with a probe radius of 1.2 Å using Mercury software (only 6.2% if the probe radius used is 1.6 Å) (Fig. 2).

3.2.2. Structure of [Cu$_2$(TFMBz)$_4$(DMSO)$_2$] (2)

3.2.2.1. Low temperature phase (100 K). Compound **2** also belongs to the triclinic crystal system, with the space group P-1. The asymmetric unit contains a Cu(II) atom, two independent TFMBz anionic ligands and one DMSO neutral ligand linked to the copper atom trough the oxygen

Table 1
Intermolecular interactions for [Cu(TFMBz)$_2$(ISNA)$_2$] (**1**).

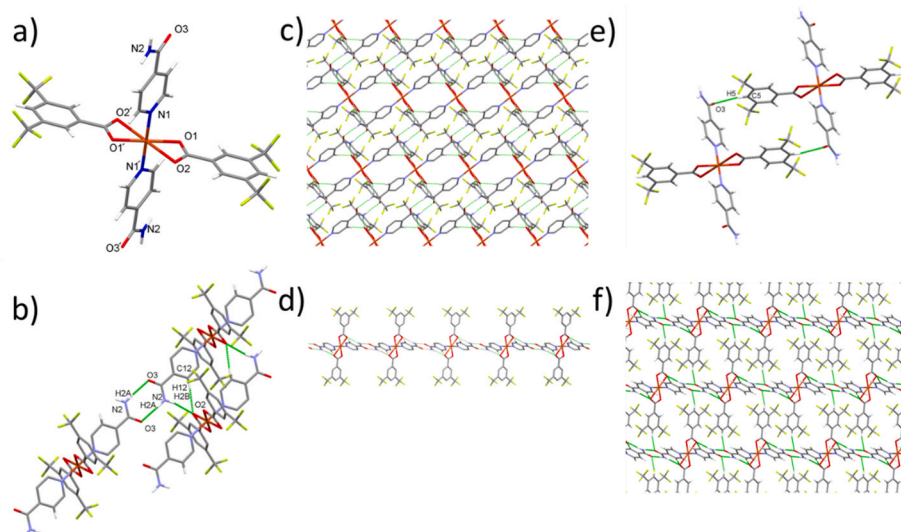| D-H⋯A	D-H (Å)	H⋯A (Å)	D⋯A (Å)	> D-H⋯A (°)
N(2)-H(2A)⋯O(3)	0.86	2.03	2.887(3)	175
N(2)-H(2B)⋯O(2)	0.86	2.04	2.885(3)	168
C(5)-H(5)⋯O(3)	0.93	2.34	3.243(3)	164
C(12)-H(12)⋯O(2)	0.93	2.25	3.157(3)	166

Fig. 1. Structure of **1**, [Cu(TFMBz)$_2$(ISNA)$_2$]: (a) molecule detail; (b) detail of the hydrogen bonds stablished by each ISNA ligand; (c) 2D supramolecular network generated by the expansion of the former hydrogen bonds (view along *c* axis); and (d) lateral view of the 2D supramolecular network. Hydrogen atoms, except those participating in intermolecular hydrogen bonds, are omitted for clarity. Depicted hydrogen bonds are denoted as dotted green lines; (e) detail of the intermolecular contacts between adjacent supramolecular 2D networks; and (f) view of the packing highlighting the former contacts.
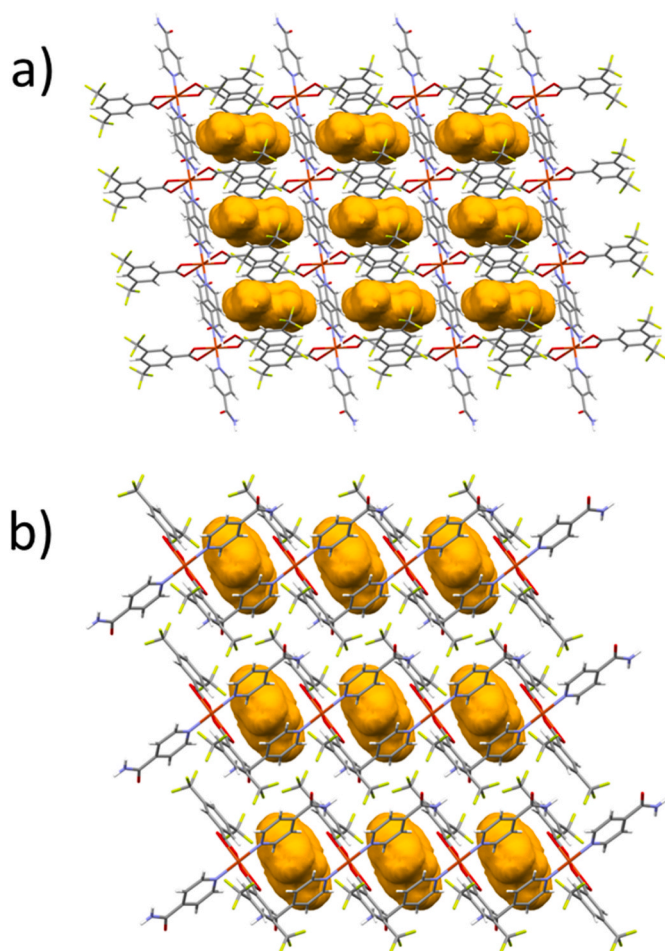
Fig. 2. Voids, determined with a probe radius of 1.2 Å (Mercury 2022.3), in the crystal structure of **1** [Cu(TFMBz)₂(ISNA)₂]: (a) view along *b* axis; and (b) view along *c* axis.

atom. This binuclear complex adopts the typical paddle wheel structure: two equivalent Cu(II) are held together by four *sin-sin* μ_2,η^1,η^1 carboxylate bridges from four TFMBz ligands, while two DMSO occupy the axial positions. All the Cu-O(carboxylate) bond lengths are in a narrow interval (1.964(2)-1.975(2) Å), while the Cu-O(DMSO) bond length is 2.101(4) Å (Fig. 3a). DMSO ligands of neighbor molecules are paired by a double hydrogen bond between H atoms of the methyl group and the O atom (O5···H20A-C20, $d_{O\cdots H}$ 2.54 Å; $d_{O\cdots C}$ = 3.386(7) Å), noticeably stronger than those observed in pure solid DMSO at the same temperature [36]. The expansion of these intermolecular hydrogen bonds defines supramolecular chains parallel to the *a* axis (Fig. 3b). These chains are interconnected by π - π intermolecular contacts in the [010] direction (centroid-centroid distances 3.556(4) Å), combined with weaker π - π interactions in the [001] direction (centroid-centroid distances 3.888(4) Å) (Fig. 3c).

As two of the four independent -CF₃ groups are disordered (two alternative positions for each fluoride atom), guest accessible space visualization is not trivial. When one of the fluoride positions is fixed to the most populated position, only non-interconnected voids are generated. Contrarily, when the less populated positions are arbitrarily fixed and the probe radius is unrealistically reduced to 1.1 Å, channels are generated (Fig. 4). In fact, the fluoride disorder suggests that the energy barrier to the rotation of half of the -CF₃ groups is still feasible at this low temperature, and probably also at 77 K, the temperature used for the N₂ adsorption-desorption isotherm measurements.

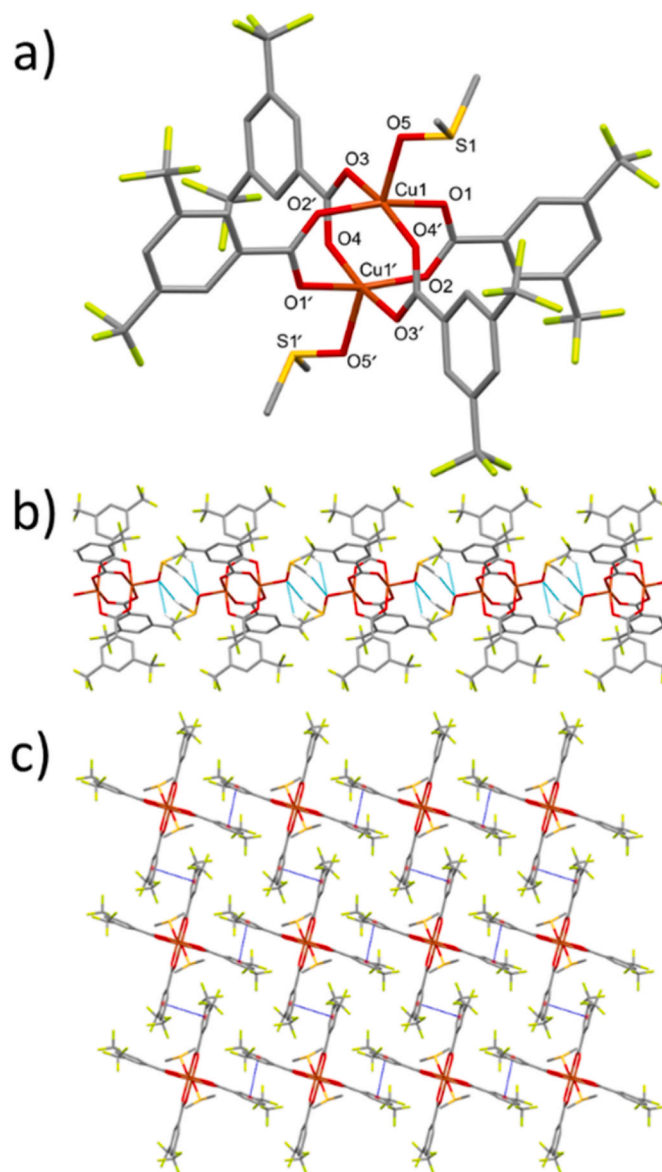*3.2.2.2. Phase change evidence and room temperature crystal structure.*

Fig. 3. Crystal structure of **2**, [Cu₂(TFMBz)₄(DMSO)₂]: (a) molecule detail; (b) detail of the stablished hydrogen bonds between adjacent molecules. Their expansion defines chains parallel to the *a* axis; (c) view of the packing along the *a* axis; π-π interactions are depicted as dotted blue lines. For clarity, hydrogen atoms, except those participating in the hydrogen bonds, are omitted for clarity and only the position most populated of each disordered fluoride atoms is depicted.

The former description is based on the determination of the structure from crystallographic data measured at 100 K. Additional information can be acquired by measuring the variable temperature SPXRD patterns of the sample. Measurements performed in the temperature interval 300 to 100 K indicated a sharp variation on the pattern at around 245 K (Fig. 5). This behavior is confirmed by DSC characterization, in which two close exothermic events are displayed at 256 and 248 K (Fig. 6). The correspondent enthalpy values are *ca.* −0.7 and −1.3 kJ/mol, respectively. These thermal events correspond to a first-order phase transitions [37]. To gain further information, structure elucidation has also been done from data obtained at room temperature. Despite the changes observed in the SPXRD patterns at *ca.* 245 K, the structure determined at room temperature is similar to the one described at 100 K. The spatial group was preserved, though, as expected due to thermal expansion, the cell volume increased in *ca.* 4.5%, while the angles varied in opposite
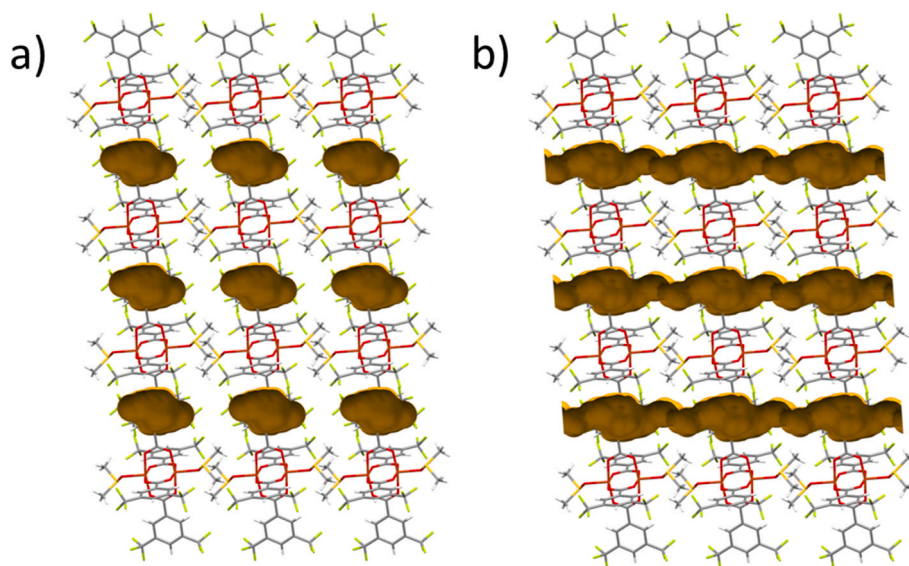
Fig. 4. Crystal packing of $[Cu_2(TFMBz)_4(DMSO)_2]$: view along c axis. Isolated voids appear with a probe radius of 1.2 Å, while the narrow channels turn up only by reducing the probe radius to 1.1 Å (Mercury 2022.3).
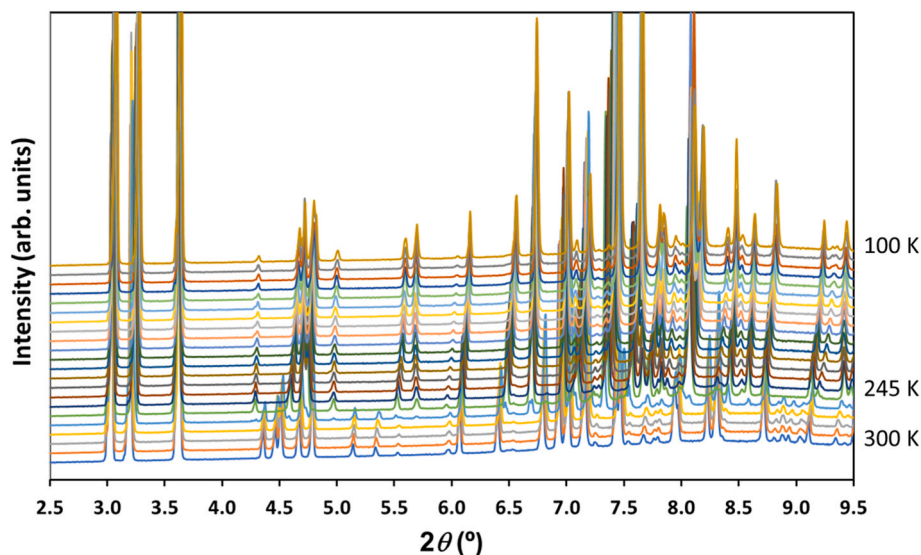

Fig. 5. SPXRD patterns at variable temperature measured under vacuum for $[Cu_2(TFMBz)_4(DMSO)_2]$ (**2**).

directions, *e.g.*, alfa increased while beta and gamma decreased. The key difference is that, at room temperature, all -CF_3 groups, and also the DMSO axial ligands, present disorder: two alternative positions for each fluoride atom in -CF_3 groups and two alternative positions for all the atoms of DMSO, except the oxygen atom linked to the metal cation. Hence, considering variable temperature SPXRD and DSC data, **2** shows a phase change at *ca.* 245 K that involves variations in the order or disorder of these parts of the molecule, half of the CF_3 and DMSO, while the other half of -CF_3 still present disorder at low temperature.

3.3. Adsorption properties

Compound **1** does not show any appreciable adsorption of N_2 at 77 K, denoting that the voids determined in the elucidated crystal structure are not accessible to guests. Conversely, **1** shows an appreciable adsorption of CO_2 at 273 K (Fig. 7), which corresponds approximately to one CO_2 molecule per copper atom, or which is the same, one CO_2 molecule per void. Although the volume of each void is large enough to

accommodate a CO_2 molecule, the analysis of the crystal structure does not show interconnection between voids to allow the diffusion of any gas. A plausible explanation to this disparity is that at 77 K the hydrogen bond supramolecular network was rigid enough to prevent the diffusion of any molecule between voids. On the contrary, at 273 K the thermal energy was enough to foster a significant level of flexibility, including vibration and rotation motions, even when that implies transient hydrogen bonding weakening or rupture. This flexibility creates transient communication between initially isolated pores, allowing the diffusion of potential guest molecules [38,39]. The isosteric heats of adsorption (Q_{st}) for compound **1** were measured as a function of CO_2 uptake (Fig. 8 and S3). The Q_{st} values varied between -28.8 kJ mol^{-1} at low coverages and -22.8 kJ mol^{-1} when the amount of adsorbed CO_2 increases. This range of values should be considered as moderate when compared to the Q_{st} values reported for standard conventional porous materials applied for CO_2 adsorption, such as microporous carbons, zeolites or MOFs [40]. The obtained Q_{st} value for **1** denotes physisorption, thus facilitating the reverse desorption process and the reuse
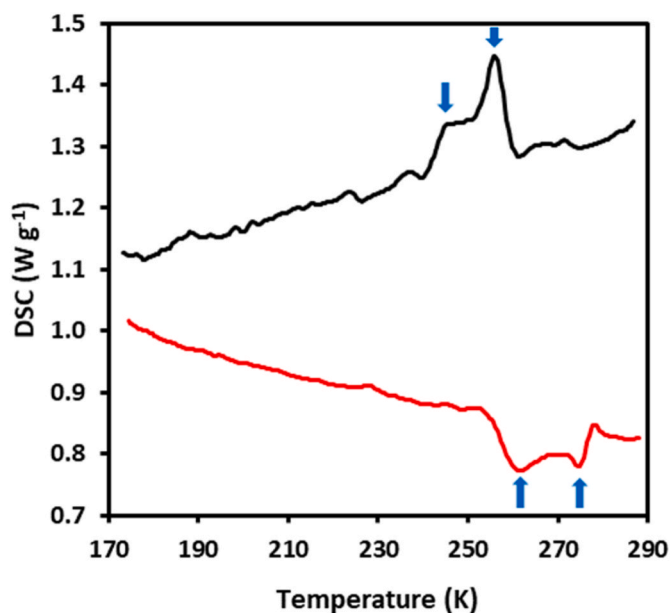
Fig. 6. DSC curves recorded for $[Cu_2(TFMBz)_4(DMSO)_2]$ (**2**) (black and red lines for cooling and heating, respectively, 5 K min^{-1}) indicating phase transitions. Peaks maximum/minimum are marked by arrows.
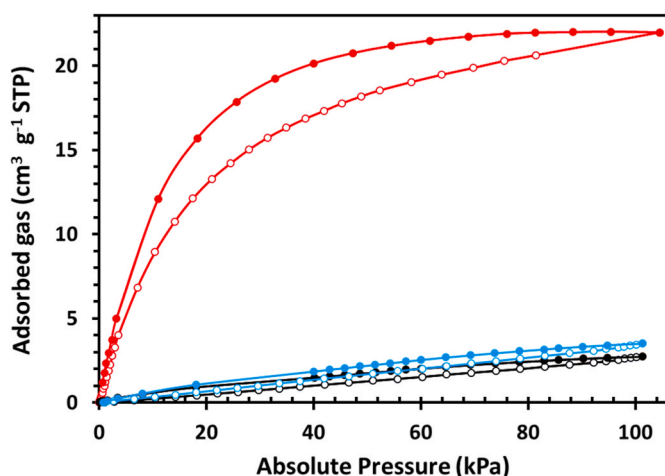

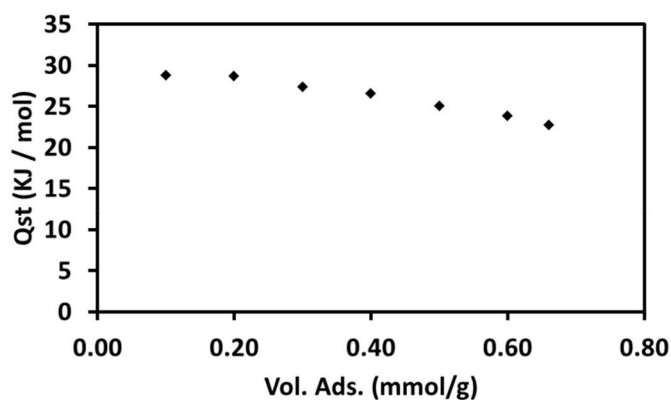**Fig. 7.** Adsorption/desorption isotherms of CO_2 (red), Ar (blue) and N_2 (black) at 273 K for $[Cu(TFMbz)_2(ISNA)_2]$ (**1**).

Fig. 8. Calculated Q_{st} values at different surface coverages of CO_2 adsorbed on $[Cu(TFMbz)_2(ISNA)_2]$ (**1**).

of the materials [41]. Nevertheless, the adsorption of N_2 or Ar at 273 K was noticeable lower than that of CO_2, denoting a significant degree of selectivity for **1** (Fig. 7). It is also remarkable that, despite the high solvent accessible volume of 133 Å^3 per unit cell according to Platon report [42], the as-synthesized **1** do not contain occluded solvent molecules (methanol or water), which also indicates a certain degree of selectivity towards potential guest.

Compound **2** shows adsorption of N_2 and Ar at 77 K (Fig. 9). The SSCXRD data analysis indicates the presence of channels, but only when using a probe radius of 1.1 Å, instead of the isolated voids observed in **1**. The need of such a small probe radius to define the channels implies that the necks are not wide enough to allow the diffusion of N_2 [43,44]. However, experimental measurements of the adsorption isotherm of N_2 in **2**, repeated several times and with different batch samples, evidenced adsorption of this gas at 77 K. Again, this implies that dynamic effects (vibrational and rotation motions) must account for the momentary widening necessary to adsorbate diffusion between voids [45]. The amount of N_2 adsorbed corresponds roughly to one N_2 molecule per void observed in Fig. 9a, or what is the same, one N_2 per adsorbate molecular unit. The measured amount of adsorbed N_2 at 100 kPa was 1.11 N_2/Cu dimer, which take into account the additional contribution to adsorption of the external surface of the adsorbate particles. It is remarkable that in
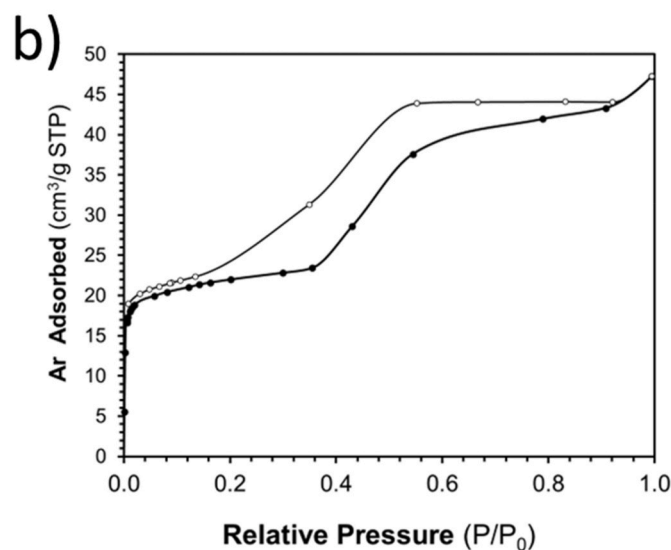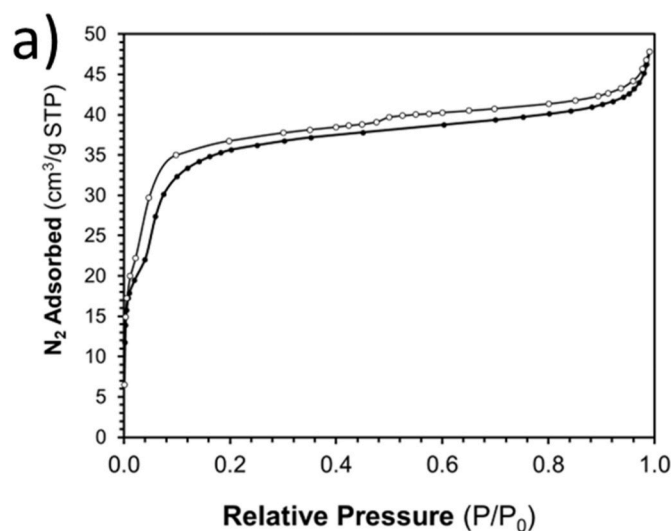

Fig. 9. Adsorption/desorption isotherms of N_2 (a) and Ar(b) at 77 K for $[Cu_2(TFMBz)_4(DMSO)_2]$ (**2**).

this case the volume of the void per unit cell (46.1 $\mathring{A}^3$ per unit cell according Platon report) [38] was very close to the volume of a N_2 molecule estimated in the liquid state (51.7 $\mathring{A}^3$). For Ar, a slightly larger amount than for N_2 was adsorbed, in the order of 1.3 Ar/Cu dimer at 100 kPa. The previously described disorder of half of the -CF$_3$ groups in the structure at 100 K suggests that to cross the energy barrier for rotation of these -CF$_3$ groups was still feasible at this low temperature, and probably also at 77 K, the temperature of the N_2 and Ar adsorption-desorption isotherms measurement. Rotation of some -CF$_3$ groups, accompanied of some vibration, etc., must contribute to create the transient channels that allow N_2 diffusion inside the solid material. The displayed N_2 and Ar isotherms for **2** (Fig. 9) only reflects equilibrium positions. However, it is remarkable that the measurements take a long time, longer than usual in a microporous compound. The fact that the time required to attain each equilibrium point is remarkably large, suggests that the diffusion of the guest is somehow sluggish. Nevertheless, the attained adsorption when related to the volume of the void is close to the limit value. The amount of adsorbed CO_2 at 273 was very low, only 0.13 CO_2/Cu dimer, and related to adsorption on the external surface of the material.

The N_2 and Ar adsorption isotherms recorded for **2** displayed some unique characteristics (Fig. 9), such as hysteresis and stepped shape. Both effects have been associated with structural changes occurring during adsorption [46,47]. This behavior can also be observed comparing the SPXRD spectra obtained under vacuum (on cooling in Fig. 5) and atmospheric conditions (Fig. S4), displaying clear differences in the two diffraction peaks around 5.7° that appear doubled at the lower temperatures diffractograms. This difference is attributed to the presence of N_2 in the experiment in which the sample holder was not submitted to vacuum during cooling. The observed changes are a combination of the effect of cooling and N_2 adsorption, especially in the lowest range of temperatures. In fact, the adsorption of N_2 during the measurements also takes place during data acquisition of single crystal X-ray diffraction at 100 K of, in which a flux of cool nitrogen is used to control de temperature, being the monocrystal of **2** in direct contact with it. The reported crystal structure was solved with the aid of the solvent masking method (note the "[+solvent]" notation in the checkcif file). Particularly, the electron density accounted with the solvent masking methodology corresponds to six electrons by unit cell. As each N_2 molecule has 14 electrons, these six electrons equal to 0.43 molecules, i. e., roughly half of the voids are filled with N_2.

This adsorption of N_2 accounts for the difference between the simulated diffractogram from the single crystal data and the ones measured under vacuum (Fig. S5, compare the black and red lines). The diffractogram of the sample cooled without applying vacuum (Fig. S5, blue line) displayed also some differences with the simulated one due to the slowness of the process of N_2 adsorption, as discussed previously. Nevertheless, when the sample is maintained under these conditions at this temperature, the N_2 adsorption continues and a diffractogram matching the simulated one is obtained (Fig. S5, green line). It is worth noting that, although the most intense peaks in the SSCXRD patterns do not experiment significative shifts, the described alterations of the lines around 5.7° clearly indicate some minor structural changes arising during the adsorption process.

4. Conclusions

Two new Cu(II)/TFMBz PMC complexes were synthetized and their structure elucidated crystallographically: the mononuclear [Cu(TFMBz)$_2$(ISNA)$_2$] (**1**) and the binuclear [Cu$_2$(TFMBz)$_4$(DMSO)$_2$] (**2**). In these two compounds, the type of established intermolecular forces and energy determine the solid-state dynamics, and, particularly, the minimum temperature necessary to allow a dynamic motion of parts of the structure (rotation, vibration, breaking and reforming hydrogen bonds, *etc*), which is necessary to allow the diffusion of adsorbates by the generation of an apparent microporous compound. The reversible

adsorption/desorption of different gases (CO_2 on **1**, and N_2 or Ar on **2**) denotes that in both PMCs different guests can diffuse through the structure, in spite that only isolated voids can be observed in the analysis of porosity performed from structural data. Experimental observations can only be rationalized considering dynamic porosity. For **2**, the hysteresis loops and stepped shape of the N_2 and Ar isotherms suggest that some small structural changes occurs concomitant with the adsorption process, observation confirmed by SPXRD characterization.

CRediT authorship contribution statement

Oriol Vallcorba: Methodology, Investigation, Formal analysis, Data curation. **Julio Fraile-Sainz:** Methodology, Investigation, Formal analysis. **Concepción Domingo:** Funding acquisition, Methodology, Project administration, Resources, Supervision, Investigation, Writing – review & editing. **José A. Ayllón:** Writing – review & editing, Writing – original draft, Supervision, Investigation, Formal analysis, Conceptualization.

Declaration of competing interest

The authors declare that they have no known competing financial interests or personal relationships that could have appeared to influence the work reported in this paper.

Data availability

Data will be made available on request.

Acknowledgements

Appendix A. Supplementary data

Supplementary data to this article can be found online at https://doi.org/10.1016/j.micromeso.2023.112688.

References

[1] R. Freund, O. Zaremba, G. Arnauts, R. Ameloot, G. Skorupskii, M. Dincă, A. Bavykina, J. Gascon, A. Ejsmont, J. Goscianska, M. Kalmutzki, U. Lächelt, E. Ploetz, C.S. Diercks, S. Wuttke, The current status of MOF and COF applications, Angew. Chem. Int. Ed. 60 (2021) 23975–24001.
[2] P. Silva, S.M.F. Vilela, J.P.C. Tomé, F.A. Almeida Paz, Multifunctional metal–organic frameworks: from academia to industrial applications, Chem. Soc. Rev. 44 (2015) 6774–6803.
[3] Z. Ji, H. Wang, S. Canossa, S. Wuttke, O.M. Yaghi, Pore chemistry of metal–organic frameworks, Adv. Funct. Mater. 30 (2020), 2000238.
[4] H. Lyu, H. Li, N. Hanikel, K. Wang, O.M. Yaghi, Covalent organic frameworks for carbon dioxide capture from air, J. Am. Chem. Soc. 144 (2022) 12989–12995.
[5] M.S. Lohse, T. Bein, Covalent organic frameworks: structures, synthesis, and applications, Adv. Funct. Mater. 28 (2018), 1705553.
[6] M.M. Deegan, M.R. Dworzak, A.J. Gosselin, K.J. Korman, E.D. Bloch, Gas storage in porous molecular materials, Chem. Eur J. 27 (2021) 4531–4547.
[7] I. Bassanetti, A. Comotti, P. Sozzani, S. Bracco, G. Calestani, F. Mezzadri, L. Marchiò, Porous molecular crystals by macrocyclic coordination supramolecules, J. Am. Chem. Soc. 136 (2014) 14883–14895.
[8] H. Yamagishi, Functions and fundamentals of porous molecular crystals sustained by labile bonds, Chem. Commun. 58 (2022) 11887–11897.
[9] N.B. McKeown, Nanoporous molecular crystals, J. Mater. Chem. 20 (2010) 10588–10597.
[10] P. Li, M.R. Ryder, J.F. Stoddart, Hydrogen-bonded organic frameworks: a rising class of porous molecular materials, Acc. Mater. Res. 1 (2020) 77–87.

[11] D. Shao, P. Peng, M. You, L.-F. Shen, S.-Y. She, Y.-Q. Zhang, Z. Tian, Hydrogen-bonded framework of a cobalt(II) complex showing superior stability and field-induced slow magnetic relaxation, Inorg. Chem. 61 (2022) 3754–3762.

[12] G. Zhang, O. Presly, F. White, I.M. Oppel, M. Mastalerz, A permanent mesoporous organic cage with an exceptionally high surface area, Angew. Chem. Int. Ed. 53 (2014) 1516–1520.

[13] L. Chen, P.S. Reiss, S.Y. Chong, D. Holden, K.E. Jelfs, T. Hasell, M.A. Little, A. Kewley, M.E. Briggs, A. Stephenson, K.M. Thomas, J.A. Armstrong, J. Bell, J. Busto, R. Noel, J. Liu, D.M. Strachan, P.K. Thallapally, A.I. Cooper, Separation of rare gases and chiral molecules by selective binding in porous organic cages, Nat. Mater. 13 (2014) 954–960.

[14] H. Sasaki, H. Imoto, T. Kitao, T. Uemura, T. Yumura, K. Naka, Fluorinated porous molecular crystals: vapor-triggered on–off switching of luminescence and porosity, Chem. Commun. 55 (2019) 6487–6490.

[15] N. Dwarkanath, S. Palchowdhury, S. Balasubramanian, Unraveling the sorption mechanism of CO_2 in a molecular crystal without intrinsic porosity, J. Phys. Chem. B 123 (2019) 7471–7481.

[16] E. Sánchez-González, M.Y. Tsang, J. Troyano, G.A. Craig, S. Furukawa, Assembling metal–organic cages as porous materials, Chem. Soc. Rev. 51 (2022) 4876–4889.

[17] M.J. Bojdys, M.E. Briggs, J.T.A. Jones, D.J. Adams, S.Y. Chong, M. Schmidtmann, A.I. Cooper, Supramolecular engineering of intrinsic and extrinsic porosity in covalent organic cages, J. Am. Chem. Soc. 133 (2011) 16566–16571.

[18] S. Noro, T. Ohba, K. Fukuhara, Y. Takahashi, T. Akutagawa, T. Nakamura, Diverse structures and adsorption properties of quasi-Werner-type copper(ii) complexes with flexible and polar axial bonds, Dalton Trans. 40 (2011) 2268–2274.

[19] A.M. Kałuża, S. Mukherjee, S.-Q. Wang, D.J. O'Hearn, M.J. Zaworotko, [Cu(4-phenylpyridine)$_4$ (trifluoromethanesulfonate) $_2$], a Werner complex that exhibits high selectivity for o-xylene, Chem. Commun. 56 (2020) 1940–1943.

[20] C. Cui, P.R. Shipman, R.A. Lalancette, F. Jäkle, Tris(2-pyridylborate) (tpyb) metal complexes: synthesis, characterization, and formation of extrinsically porous materials with large cylindrical channels, Inorg. Chem. 52 (2013) 9440–9448.

[21] B. Kohl, F. Rominger, M. Mastalerz, Crystal structures of a molecule designed not to pack tightly, Chem. Eur J. 21 (2015) 17308–17313.

[22] E. Coropceanu, A. Rija, V. Lozan, I. Bulhac, G. Duca, V.Ch Kravtsov, P. Bourosh, Discrete binuclear cobalt(III) bis-dioximates with wheel-and-axle topology as building blocks to afford porous supramolecular metal–organic frameworks, Cryst. Growth Des. 16 (2016) 814–820.

[23] A. Bacchi, P. Pelagatti, Fabricating organometallic wheel-and-axle compounds for the creation of dynamically porous crystalline materials, CrystEngComm 18 (2016) 6114–6123.

[24] D. Holden, S.Y. Chong, L. Chen, K.E. Jelfs, T. Hasell, A.I. Cooper, Understanding static, dynamic and cooperative porosity in molecular materials, Chem. Sci. 7 (2016) 4875–4879.

[25] J.L. Atwood, L.J. Barbour, A. Jerga, B.L. Schottel, Guest transport in a nonporous organic solid via dynamic van der Waals cooperativity, Science 298 (2002) 1000–1002.

[26] S. Noro, Y. Meng, K. Suzuki, M. Sugiura, Y. Hijikata, J. Pirillo, X. Zheng, K. Takahashi, T. Nakamura, A temporarily pore-openable porous coordination polymer for guest adsorption/desorption, Inorg. Chem. 60 (2021) 4531–4538.

[27] L.J. Barbour, Crystal porosity and the burden of proof, Chem. Commun. (2006) 1163–1168.

[28] L. Dobrzańska, G.O. Lloyd, H.G. Raubenheimer, L.J. Barbour, Permeability of a seemingly nonporous crystal formed by a discrete metallocyclic complex, J. Am. Chem. Soc. 128 (2006) 698–699.

[29] F. Papi, A. Rosado, O. Vallcorba, A.E. Lanza, M. Gemmi, N. Portolés-Gil, A. M. López-Periago, C. Domingo, J.A. Ayllón, Supramolecular isomerism in cobalt(II) coordination polymers built from 3,5-Bis(trifluoromethyl)benzoate and 4,4'-bipyridine, Cryst. Growth Des. 22 (2022) 4463–4471.

[30] J. Juanhuix, F. Gil-Ortiz, G. Cuní, C. Colldelram, J. Nicolás, J. Lidón, E. Boter, C. Ruget, S. Ferrer, J. Benach, Developments in optics and performance at BL13-XALOC, the macromolecular crystallography beamline at the Alba Synchrotron, J. Synchrotron Radiat. 21 (2014) 679–689.

[31] W. Kabsch, XDS, Acta Crystallogr D Biol Crystallogr 66 (2010) 125–132.

[32] G.M. Sheldrick, Crystal structure refinement with *SHELXL*, Acta Crystallogr C Struct Chem 71 (2015) 3–8.

[33] O.V. Dolomanov, L.J. Bourhis, R.J. Gildea, J.A.K. Howard, H. Puschmann, *OLEX2* : a complete structure solution, refinement and analysis program, J. Appl. Crystallogr. 42 (2009) 339–341.

[34] C.B. Aakeröy, A.M. Beatty, J. Desper, M. O'Shea, J. Valdés-Martínez, Directed assembly of dinuclear and mononuclear copper(ii)-carboxylates into infinite 1-D motifs using isonicotinamide as a high-yielding supramolecular reagent, Dalton Trans. (2003) 3956–3962.

[35] F. Sánchez-Férez, L. Bayés, M. Font-Bardia, J. Pons, Solvent dependent formation of Cu(II) complexes based on isonicotinamide ligand, Inorg. Chim. Acta. 494 (2019) 112–122.

[36] H. Reuter, Structural parameters of dimethyl sulfoxide, DMSO, at 100 K, based on a redetermination by use of high-quality single-crystal X-ray data, Acta Crystallogr E Cryst Commun 73 (2017) 1405–1408.

[37] L. Yuan, S. Clevers, A. Burel, P. Negrier, M. del Barrio, B. Ben Hassine, D. Mondieig, V. Dupray, J.Ll Tamarit, G. Coquerel, New intermediate polymorph of 1-Fluoro-adamantane and its second-order-like transition toward the low temperature phase, Cryst. Growth Des. 17 (2017) 3395–3401.

[38] A. Aguilar-Granda, S. Pérez-Estrada, E. Sánchez-González, J.R. Álvarez, J. Rodríguez-Hernández, M. Rodríguez, A.E. Roa, S. Hernández-Ortega, I.A. Ibarra, B. Rodríguez-Molina, Transient porosity in densely packed crystalline carbazole–(p-Diethynylphenylene)–Carbazole rotors: CO_2 and acetone sorption properties, J. Am. Chem. Soc. 139 (2017) 7549–7557.

[39] M. Inukai, M. Tamura, S. Horike, M. Higuchi, S. Kitagawa, K. Nakamura, Storage of CO_2 into porous coordination polymer controlled by molecular rotor dynamics, Angew. Chem. Int. Ed. 57 (2018) 8687–8690.

[40] M. Oschatz, M. Antonietti, A search for selectivity to enable CO_2 capture with porous adsorbents, Energy Environ. Sci. 11 (2018) 57–70.

[41] M. Khraisheh, S. Mukherjee, A. Kumar, F. Al Momani, G. Walker, M.J. Zaworotko, An overview on trace CO2 removal by advanced physisorbent materials, J. Environ. Manag. 255 (2020), 109874.

[42] A.L. Spek, Single-crystal structure validation with the program *PLATON*, J. Appl. Crystallogr. 36 (2003) 7–13.

[43] D. Ongari, P.G. Boyd, S. Barthel, M. Witman, M. Haranczyk, B. Smit, Accurate characterization of the pore volume in microporous crystalline materials, Langmuir 33 (2017) 14529–14538.

[44] M. Wu, M. Li, L. Yuan, F. Pan, "Useless channels" in a molecular crystal formed via F···F and F···π halogen bonds, Cryst. Growth Des. 22 (2022) 971–975.

[45] T. Kurihara, M. Inukai, M. Mizuno, Slow CO_2 diffusion governed by steric hindrance of rotatory ligands in small pores of a metal–organic framework, J. Phys. Chem. Lett. 13 (2022) 7023–7028.

[46] F.-X. Coudert, J.D. Evans, Nanoscale metamaterials: meta-MOFs and framework materials with anomalous behavior, Coord. Chem. Rev. 388 (2019) 48–62.

[47] Q. Yang, P. Lama, S. Sen, M. Lusi, K. Chen, W. Gao, M. Shivanna, T. Pham, N. Hosono, S. Kusaka, J.J. Perry, S. Ma, B. Space, L.J. Barbour, S. Kitagawa, M. J. Zaworotko, Reversible switching between highly porous and nonporous phases of an interpenetrated diamondoid coordination network that exhibits gate-opening at methane storage pressures, Angew. Chem. Int. Ed. 57 (2018) 5684–5689.